Geophysical Prospecting, 1999, 47, 611–636

Filter formulation and wavefield separation of cross-well seismic data[1]

Jérôme Mars,[2] James W. Rector III[3] and Spyros K. Lazaratos[4]

Abstract

Multichannel filtering to obtain wavefield separation has been used in seismic processing for decades and has become an essential component in VSP and cross-well reflection imaging. The need for good multichannel wavefield separation filters is acute in borehole seismic imaging techniques such as VSP and cross-well reflection imaging, where strong interfering arrivals such as tube waves, shear conversions, multiples, direct arrivals and guided waves can overlap temporally with desired arrivals. We investigate the effects of preprocessing (alignment and equalization) on the quality of cross-well reflection imaging wavefield separation and we show that the choice of the multichannel filter and filter parameters is critical to the wavefield separation of cross-well data (median filters, f–k pie-slice filters, eigenvector filters). We show that spatial aliasing creates situations where the application of purely spatial filters (median filters) will create notches in the frequency spectrum of the desired reflection arrival. Eigenvector filters allow us to work past the limits of aliasing, but these kinds of filter are strongly dependent on the ratio of undesired to desired signal amplitude. On the basis of these observations, we developed a new type of multichannel filter that combined the best characteristics of spatial filters and eigenvector filters. We call this filter a 'constrained eigenvector filter'. We use two real data sets of cross-well seismic experiments with small and large well spacing to evaluate the effects of these factors on the quality of cross-well wavefield separation. We apply median filters, f–k pie-slice filters and constrained eigenvector filters in multiple domains available for these data sets (common-source, common-receiver, common-offset and common-midpoint gathers). We show that the results of applying the constrained eigenvector filter to the entire cross-well data set are superior to both the spatial and standard eigenvector filter results.

Introduction

Multichannel filtering to obtain wavefield separation has been used in seismic processing for decades and has become an essential component in VSP and cross-well

[1] Received May 1995, revision accepted January 1999.
[2] CEPHAG-ENSIEG, BP 46, 38402 Saint-Martin d'Hères Cedex, France.
[3] University of California, Berkeley, CA 94720, USA.
[4] TomoSeis Inc., 1650 N Sam Houston Parkway W, Houston, TX 77043, USA.

reflection imaging (Hardage 1985; Rector *et al.* 1995). The need for good multichannel wavefield separation filters is acute in borehole seismic imaging techniques such as VSP and cross-well reflection imaging, where strong interfering arrivals can overlap temporally with desired arrivals. For example, tube waves can be very strong in VSP and cross-well data. Tube waves can have a similar frequency content to the desired reflections making them difficult to attenuate temporally. Shear conversions can also be an interference problem in many wide-angle imaging applications. In conventional surface seismic data, multichannel filtering prior to stacking is often less critical because there is often a time window where reflections and multiples can be isolated. In many land surveys, ground roll can be removed by low-cut filtering in the time domain.

Previous work in VSP wavefield separation has focused on the algorithmic formulation of the wavefield separation filter and has emphasized removal of the direct arrival. Techniques such as median filters (Hardage 1985), radon filters (Foster and Mosher 1992), spectral matrix filtering (Glangeaud and Mari 1994) and optimal array filters (Seeman and Horowicz 1983) have all been advocated and explored. In cross-well reflection imaging, the volume of seismic data is often equivalent to 10 000 offset VSPs (Rector *et al.* 1995). The multiple domains available for processing (common-receiver gather, common-source gather, common-midpoint gather, common-offset gather) have dictated a more pragmatic approach in which domain selection (Rector *et al.* 1994; Rowbotham and Goulty 1994) and sequence development (Rector *et al.* 1995) have overshadowed the algorithmic formulation of the wavefield separation filter. Due to the large amount of data in cross-well reflection imaging and the great number of waves, the choice of a parametric filter processing (Esmersoy 1990) which requires heavy computation time, good signal-to-noise ratios and modelling seems to be unrealistic. Previous to our work, only simple mean filters, median filters and f–k filters had been applied to separate cross-well reflections. In addition, cross-well reflection arrivals are often contaminated by many different arrivals including tube waves, shear conversions, multiples, direct arrivals and guided waves, and therefore the multichannel filter formulations may vary with arrival type. Finally, the high frequencies present in many cross-well data (up to 2000 Hz in many cases) require very fine spatial sampling to avoid spatial aliasing. In many cases, cost considerations result in somewhat aliased data, further compounding the difficulty of wavefield separation.

We investigate the effects of three factors on the quality of cross-well reflection imaging wavefield separation:

1 Alignment and equalization of the arrival that is to be attenuated.
2 Algorithmic formulation.
3 Aliasing consideration.

We use two real data sets to evaluate the effects of these factors on the quality of cross-well wavefield separation. The first data set is a common-source gather from a West Texas carbonate environment at a small well spacing (184 ft), and the second is a complete data set from a combination clastic and carbonate sequence at British

Petroleum's Devine test site at a large well spacing (990 ft). We find that all three of the factors listed above are very crucial to the reflection imaging quality, coherence and bandwidth.

Description of multichannel filters

We tested four different types of multichannel filter on all our cross-well data sets:

1 Median filter.
2 *f–k* pie-slice filter.
3 Radon filter.
4 Eigenvector filters and constrained eigenvector filters.

The three first filters are probably the most widely used in seismic data processing. We propose adapting the eigenvector filter as a constrained eigenvector, combining the characteristics of spatial filters and the eigenvector filter.

Median filter

Median filters are the most common type of filter used in wavefield separation of VSP data. There are two important factors that make median filters attractive for wavefield separation of VSP and cross-well data. First, median filters theoretically preserve step functions or strong discontinuities and therefore do not smear reflection arrivals past their termination at the direct arrival. Second, median filters are less sensitive to outliers than mean filters and in situations where there is high amplitude crossing interference, median filters can often attenuate the interference substantially. Therefore, a median filter is ideal for eliminating noise spikes. In situations where the amplitude of the desired and undesired energy does not vary across the array, the median filter is identical to a mean filter (Duncan and Beresford 1995), which can be represented in the t–x domain as convolution with Rect(x/N), where N is the length of the filter. In the wavenumber domain, this filter is a sinc function with a main lobe half-width of $1/2N$. By changing the length of the filter we change the first zero-crossing of the filter. The main problem with this type of filter formulation is that there is no frequency dependence in the filter impulse response. This type of filter will tend to attenuate the desired signal at low frequencies. If we make the filter longer to avoid attenuating the lower frequencies, we do not reject as much of the interference at the high frequencies.

f–k *pie-slice filter*

f–k pie-slice filters are probably the most common type of multichannel filter used in surface seismic data processing (Embree, Burg and Backus 1963; Hardage 1985). In contrast to median filters, in *f–k* pie-slice filters the *k*-width of the filter increases with increasing frequency. Unlike the median filter and mean filter, which are basically wavenumber filters, *f–k* pie-slice filters are velocity filters. There are several drawbacks to the *f–k* filters. Because the filter is based on the Fourier transform, limited aperture

ensembles can have significant bin smearing in k-space. Binning can create steps in 2D filter cut-offs from which time- and space-domain ringing can result. 2D pie-slice filter tapers can be difficult to formulate. To some extent, maximum likelihood 2D spectral estimation techniques can reduce the binning problem. In addition, the linear nature of the f–k filter may be less optimal than the non-linear median filter.

Radon filter

The linear radon transform of a single common-receiver gather $r(z,t)$ can be defined as

$$\mathbf{R}(\tau, p) = \sum_j r(j\Delta z, t + p_j \Delta z),$$

where Δz is the source sampling interval and p denotes the slowness (the inverse of apparent velocity in the gather). In its hyperbolic form, the radon filter is used as a multiple suppression filter (Yilmaz 1987). A linear radon or τ–p filter is very similar to the f–k filter. A 1D filter based on p, or slowness, is theoretically identical to a pie-slice filter in f–k space. However, in the τ–p transform, the user can choose the p-domain bin size. Consequently, bin smearing is less of a problem in radon filters than in f–k filters. Additionally, filter tapers are 1D functions (of p) and are easier to formulate.

Eigenvector filter

The eigenvector filter has recently become popular in some circles as a wavefield separation technique for VSP and cross-well data (Freire and Ulrych 1988; Hardage 1992; Mars and Rector 1995). The eigenvectors of a particular gather, i.e. the function $r(t, x)$ in the t–x domain, is obtained as follows:

1 The covariance matrix $\mathbf{M}$ is computed. Each column of the covariance matrix is simply the average of the adjacent trace cross-correlation functions. The basic idea of the covariance matrix is to enhance those arrivals that are of large amplitude and are aligned or have linear moveout and to attenuate those arrivals that are either very weak and/or have static shifts between traces.

2 The singular value decomposition of $\mathbf{M}$ is computed using $\mathbf{M} = \mathbf{U}\mathbf{\Delta}\mathbf{V}^{\mathrm{T}}$, where $\mathbf{\Delta}$ is a diagonal matrix of eigenvalues, $\mathbf{U}$ is the matrix of eigenvectors of $\mathbf{M}$, and $\mathbf{V}^{\mathrm{T}}$ is the matrix of the eigenvectors of $\mathbf{M}^{\mathrm{T}}$.

3 Filtering is performed by projecting the eigenvectors corresponding to a selected number of eigenvalues on to the original gather. The eigenvectors associated with the largest eigenvalues have the most linear moveout and/or have the largest amplitude components of the original gather.

Since the eigenvector filter works on amplitude as well as moveout, it is not simply a spatial filter. A very high amplitude impulsive event would be still found in the first few eigenvectors, whereas this event would be smeared over the entire f–k plane and would not be separable with a spatial filter. Similarly, a strongly aliased, large amplitude event would be found and would possibly be separable from the desired signal in the first few

eigenvectors, whereas this event would be wrapped multiple times across the spatial Nyquist axis and would not be separable with a spatial filter. Thus, an eigenvector filter can be thought of as a filter that can attenuate large amplitude energy even when the energy has complex spatial characteristics. Eigenvector filters may be useful in attenuating large amplitude aliased arrivals such as tube waves in cross-well data sets.

One of the problems with the eigenvector filter is that it does not have an impulse response. We found that in data sets having signal-to-noise ratios that can vary as a function of trace number and time, the higher eigenvalues can often contain some components of the desired signal as well as noise. As a result of these observations, we developed a constrained eigenvector filter, which cascades a spatial filter with the eigenvector projection. By cascading a spatial filter on top of the eigenvectors, we constrain the eigenvector to attenuate only the aligned interferences.

A cross-well common-source gather case (small well spacing)

Our first data set is a single cross-well common-source gather (Fig. 1) from the

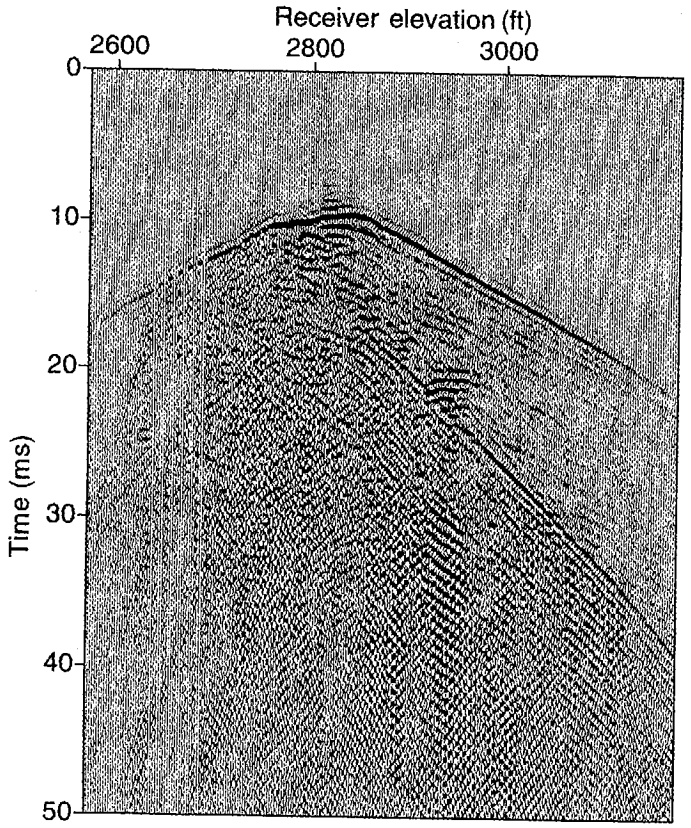

Figure 1. Cross-well common-source gather from the McElroy West Texas site.

McElroy West Texas experiment where the well spacing was 184 ft (Harris *et al.* 1995). The piezo-electric bender source was chirped from 200 to 2000 Hz and it was positioned at 2820 ft. The hydrophone receiver was moved continuously from 3150 ft to 2575 ft and sampled at 2.5 ft intervals. The small sampling interval resulted in limited spatial aliasing, primarily of the tube wave (above 1100 Hz) and the P-to-S conversions and shear arrivals (above 1600 Hz). At least 10 different arrivals were identified in the elastic modelling of a nearby common-source gather obtained by Van Schaack *et al.* (1995) and, as a result, the entire wavefield separation processing consisted of cascaded multichannel filters (Rector *et al.* 1995). In the following analysis we will focus on removal of the P- and S-wave direct arrivals (the two strongest events), and its effect on the bandwidth and the coherence of the S-wave reflections from this common-source gather.

Effect of arrival alignment and amplitude scaling

The f–k spectrum of the common-source gather is shown in Fig. 2. Although the direct arrival is roughly hyperbolic, small arrival statics and shifts in slope at velocity contrasts create an f–k spectrum where the direct arrivals smear across a large fraction of the total 2D spectrum. By contrast, the up- and downgoing tube waves travel with a roughly constant velocity and therefore exhibit a smaller range of apparent velocities in the f–k spectrum. The tube wave can be seen to wrap around the Nyquist wavenumber at about 1100 Hz. Figure 3 shows the f–k spectrum after P-wave direct arrival alignment. Alignment is well-known as an essential component in VSP and cross-well wavefield separation (Hardage 1985; Rector and Mars 1995). After alignment, the P-wave direct arrival is concentrated in a narrower range of apparent velocities. Since the P-wave direct arrival was flattened, the energy is concentrated along the $k=0$ axis or the infinite velocity.

After this first preprocessing, we use an amplitude scaling in order to enhance the flattened arrival. Figure 4 shows the data after alignment of the P-wave direct arrival and normalization of each trace by computing a scalar from a 5 ms window around the flattened direct arrival. Although perhaps less important than arrival alignment, scaling has concentrated the P-wave direct arrival into a still smaller zone around $k=0$. Amplitude variations from trace to trace in fluid-coupled cross-well data have been observed to be of up to two orders of magnitude (Rector *et al.* 1994). Without scaling, these amplitude variations produce a step-like response along the spatial axis, resulting in some smearing into all spatial frequencies. After scaling, the step-like nature of the amplitude along the spatial axis has been reduced. At this stage, a narrow filter can be applied along the $k=0$ axis to remove most of the aligned and scaled arrival. However, assuming that the desired reflection arrivals have *not* been appropriately aligned and scaled, the reflection arrivals have some components at all spatial frequencies and *any* multichannel filter that is applied will also remove some of the desired arrival energy. Therefore it is important to make the rejection filter as narrow as possible, i.e. a notch filter response.

as 184 ft (Harris *et al.* 1995).
00 to 2000 Hz and it was
ed continuously from 3150 ft
ampling interval resulted in
ve 1100 Hz) and the P-to-S
st 10 different arrivals were
urce gather obtained by Van
efield separation processing
95). In the following analysis
ls (the two strongest events),
S-wave reflections from this

in Fig. 2. Although the direct
in slope at velocity contrasts
ss a large fraction of the total
waves travel with a roughly
apparent velocities in the f–k
the Nyquist wavenumber at
vave direct arrival alignment.
SP and cross-well wavefield
alignment, the P-wave direct
velocities. Since the P-wave
along the $k=0$ axis or the

ling in order to enhance the
of the P-wave direct arrival
m a 5 ms window around the
an arrival alignment, scaling
smaller zone around $k=0$.
d cross-well data have been
t *al.* 1994). Without scaling,
ong the spatial axis, resulting
g, the step-like nature of the
stage, a narrow filter can be
and scaled arrival. However,
n appropriately aligned and
l spatial frequencies and *any*
of the desired arrival energy.
rrow as possible, i.e. a notch

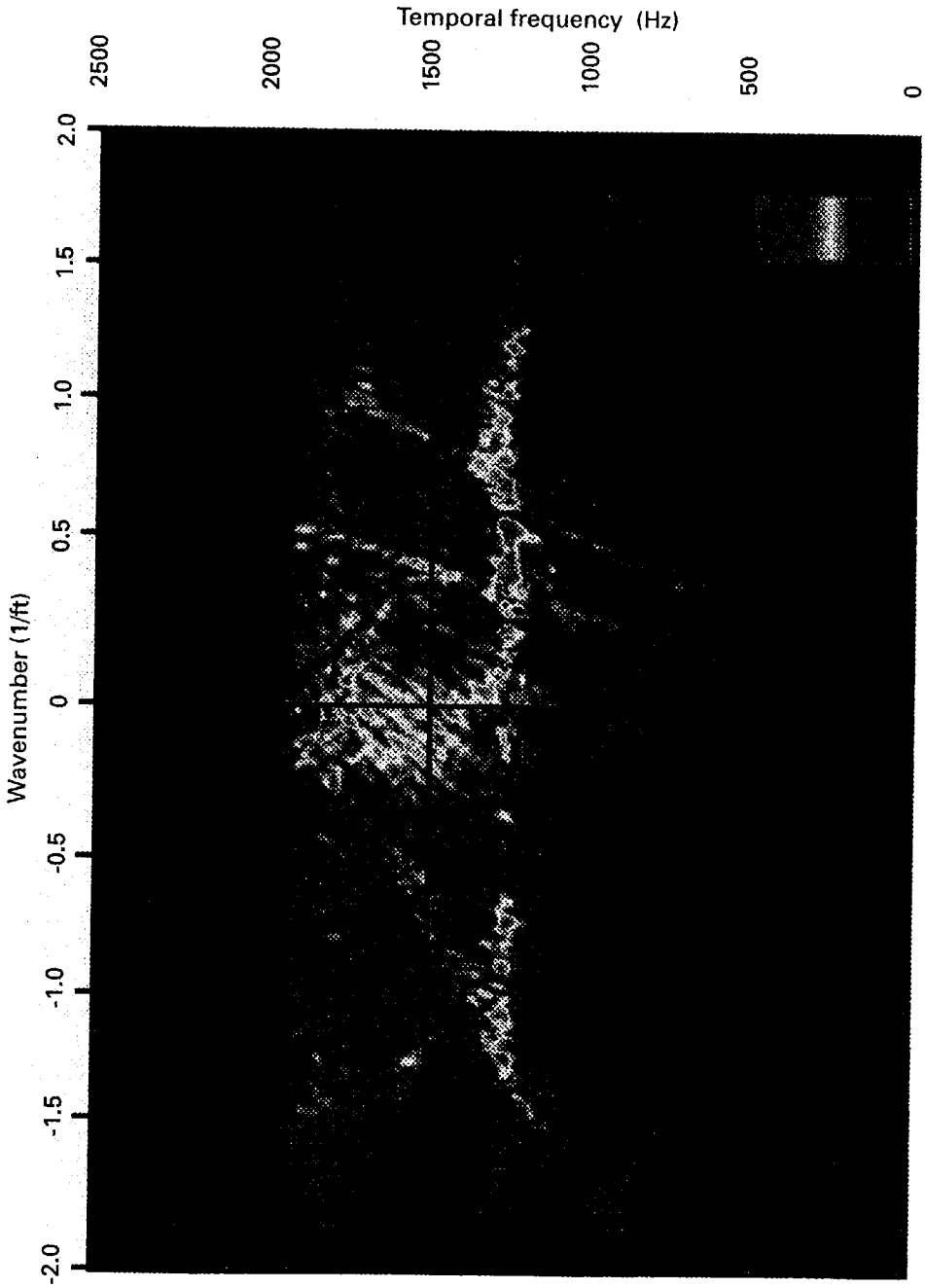

Figure 2. f–k spectrum of the initial data. P- and S-wave direct arrivals and tube waves are visible.

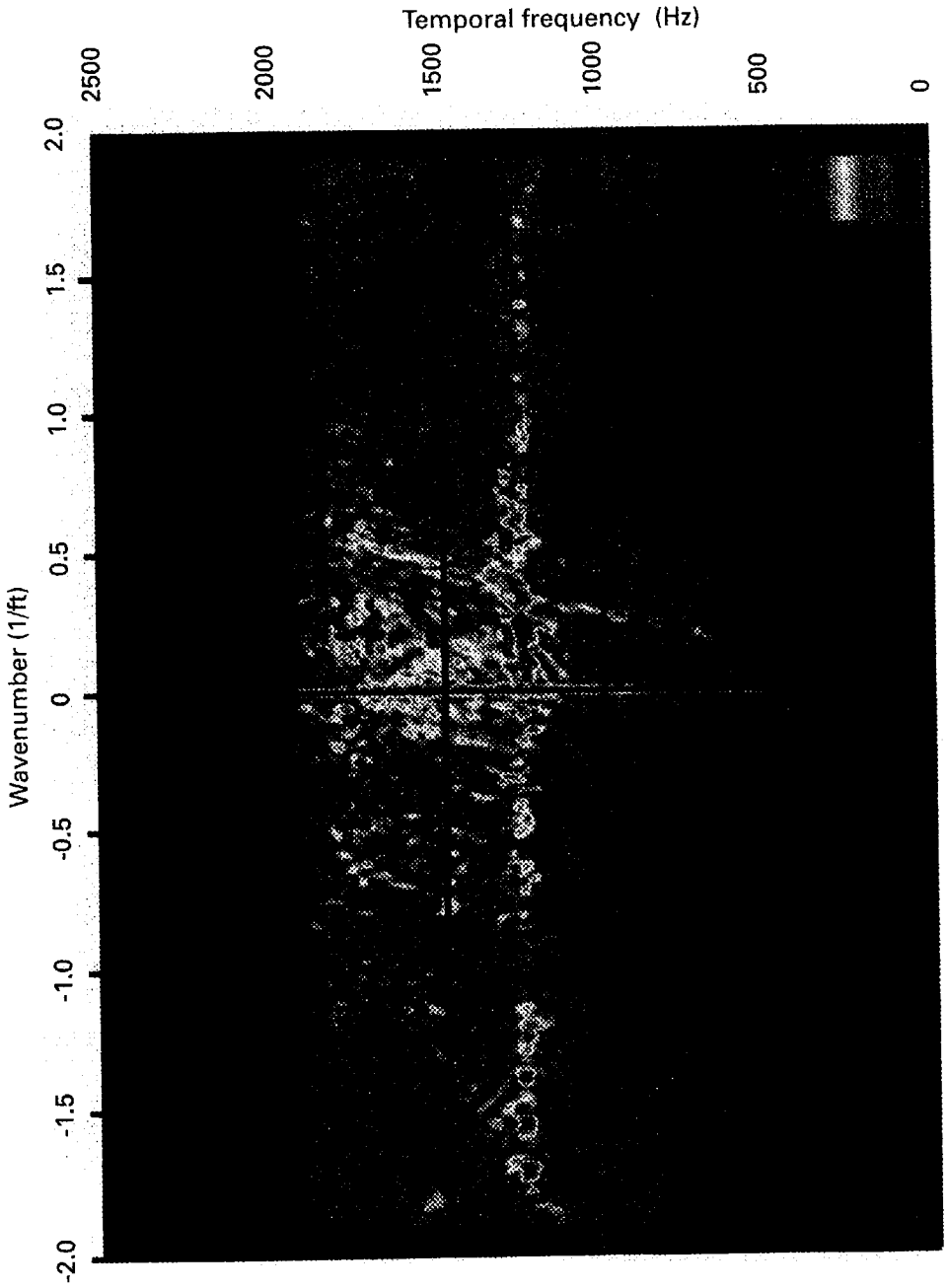

Figure 3. f–k spectrum of the initial data after alignment of the P-wave direct arrival.

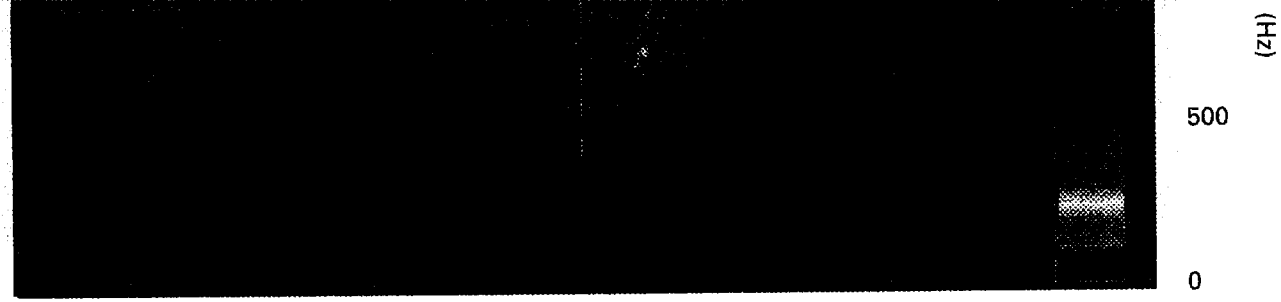

Figure 3. f–k spectrum of the initial data after alignment of the P-wave direct arrival.

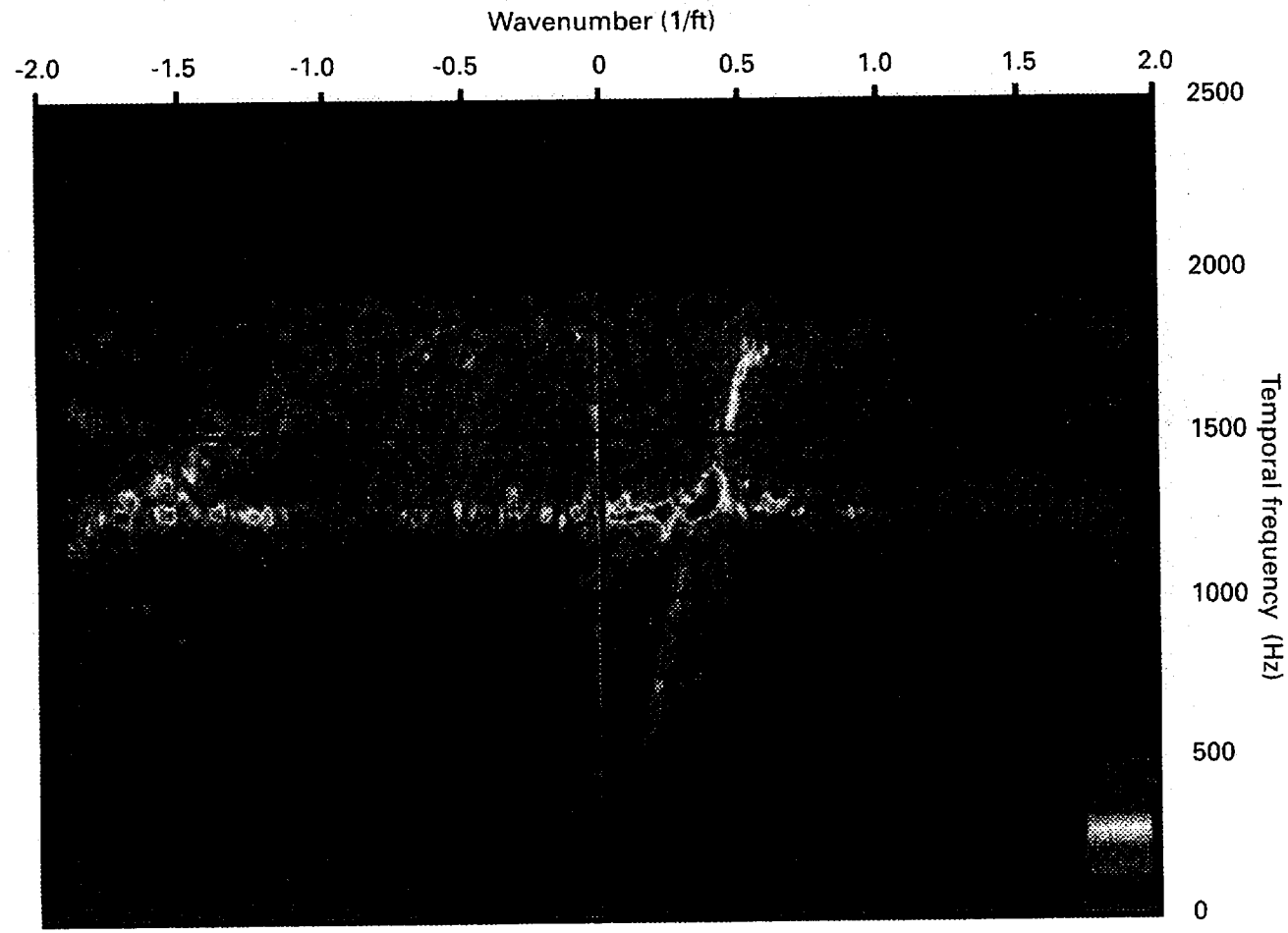

Figure 4. f–k spectrum of the initial data after alignment of the P-wave direct arrival and normalization by equalization of each trace using a 5 ms window around the P-wave direct arrival.

Geophysical Prospecting, 47, 611–636

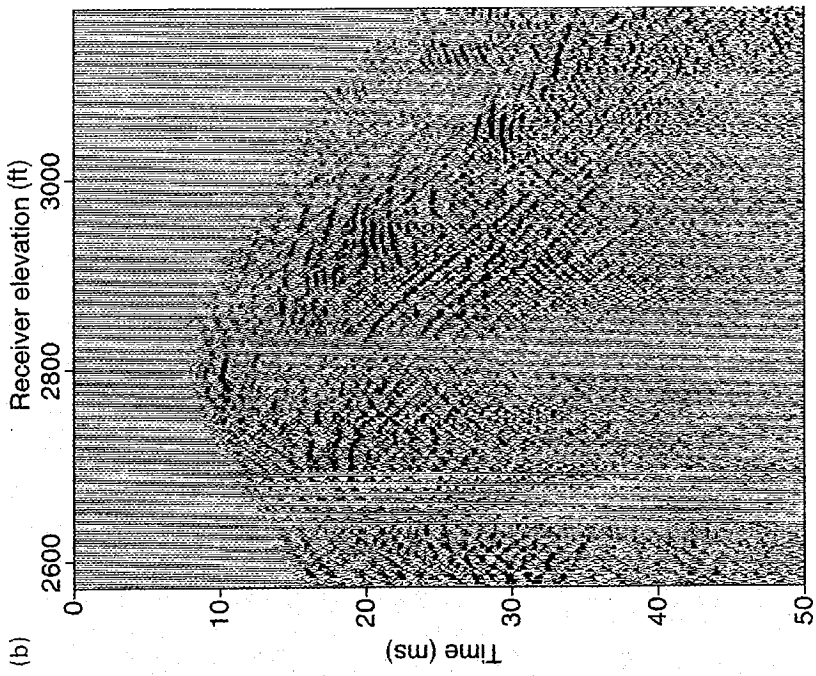
(b)
Receiver elevation (ft)
2600
2800
3000
0
10
20
30
40
50
Time (ms)

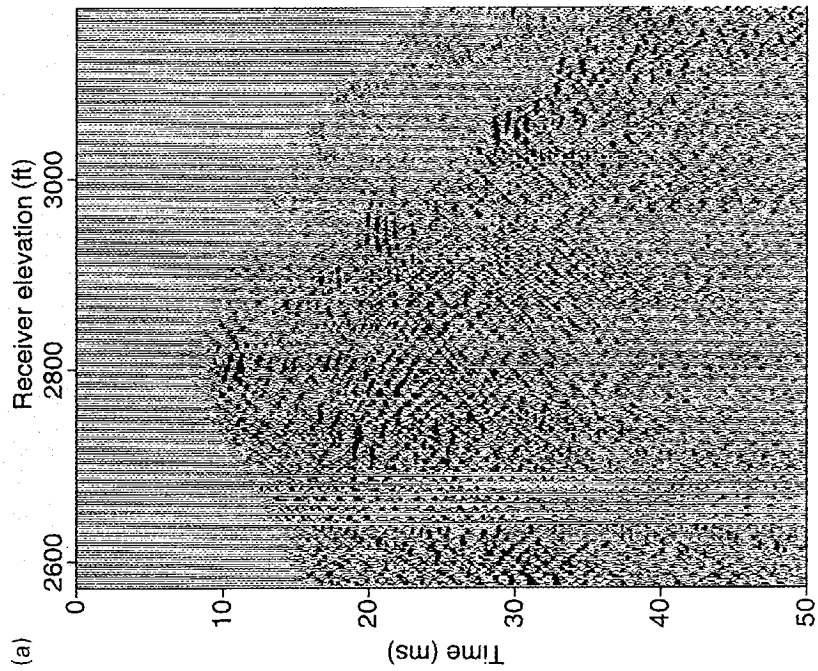
(a)
Receiver elevation (ft)
2600
2800
3000
0
10
20
30
40
50
Time (ms)

Figure 5. (a) Result obtained after removing P- and S-wave direct arrivals by median filter. (b) Result obtained after removing P- and S-wave direct arrivals by f–k pie-slice filter. (c) Result obtained after removing P- and S-wave direct arrivals by eigenvector filter. (d) Result obtained after removing P- and S-wave direct arrivals by radon filter.

Analysis of the filtered common-source gather (McElroy data)

We compared the common-source gather after two multichannel operations on it. The first removed the P-wave direct arrival by applying alignment and scaling, the second removed the S-wave direct arrival using alignment and scaling. For the median filter, we used nine traces. For the f–k and radon filters, we used a cut-off apparent velocity of $\pm$ 80 Kft/s. The slope of the fan filter was adjusted in order to remove energy around 1200 Hz (the level of maximum energy). No filter tapers were applied to any of the filters. The total percentage of the f–k spectrum removed by the f–k and radon filters was about 20%. Although there is no true analogy with the eigenvector filter, we decided to remove the largest 20% of the energy from the data as this was the percentage removed by the f–k and radon filters. In order to compare our different filters, we examined the filtered gathers in two ways. Firstly, we scrutinized plots in the x–t domain and secondly, we focused on the effect on the shear-wave attenuation in the frequency domain.

In the x–t domain (Figs 5a–d), each filter appeared to be quite effective at removing the direct arrivals, but the residual wavefields exhibit differences. The residual wavefield obtained after using the median filter is quite different from the residual wavefields obtained from the other techniques, where only minor differences were observed. The residual wavefield obtained using the median filter has significantly lower levels of P–S–P transmitted conversions and S-wave reflections. As a consequence, the P-wave reflection wavefield actually appears to be a little cleaner, particularly at the wider angles of incidence (receiver elevation: 2822.5–2947.5 ft).

Figure 6 shows the coherence between the raw data and the output of each of the multichannel filters after stacking each along the trajectory of the shear-wave reflections on receiver elev. 2822–2945. By computing a coherence function between the reflection arrivals before and after the filter application, we can evaluate what part of the reflection spectrum has been changed. Based on this result, it appears that the median filter tends to have too wide a velocity reject band at the low frequencies, and too narrow a band at the high frequencies. Consequently, the median filter acts as a sort of high-pass filter. Figure 6 confirms the low-cut, high-pass nature of the median filter. In this figure, the coherence scale is labelled as a coefficient of coherence between 0 and 1. It is a frequency-domain concept defined by $P_{ij}/\sqrt{(P_{ii}.\ P_{jj})}$, where P_{ii} and P_{jj} are power spectra and P_{ij} the cross-power spectra. The coherence between the filtered data and the raw data is nearly 1 over the frequency range from 500 to 2000 Hz for the f–k, radon and eigenvector filters. The median filter exhibits a 'low' coherence level (≤ 0.8) above 875 Hz. We did not use frequencies below 500 Hz, because the piezo-electric source used in this experiment output very weak energy in this frequency band. In essence, the reflection arrivals after median filtering have a spectrum that has little more than one octave. The other filters produce a reflection wavefield with two octaves. Perhaps a more compelling display is the inverse Fourier transform of the coherence function shown in Fig. 7. (All plots are normalized by the eigenvector filter maximum value.) The f–k, radon and eigenvector filters all yield a wavelet that is impulse-like,

a)

channel operations on it. The
ment and scaling, the second
scaling. For the median filter,
a cut-off apparent velocity of
der to remove energy around
rs were applied to any of the
d by the *f–k* and radon filters
th the eigenvector filter, we
m the data as this was the
der to compare our different
dy, we scrutinized plots in the
shear-wave attenuation in the

pe quite effective at removing
it differences. The residual
different from the residual
only minor differences were
edian filter has significantly
S-wave reflections. As a
ppears to be a little cleaner,
vation: 2822.5–2947.5 ft).
nd the output of each of the
ajectory of the shear-wave
coherence function between
n, we can evaluate what part
his result, it appears that the
d at the low frequencies, and
he median filter acts as a sort
ss nature of the median filter.
t of coherence between 0 and
$_{ii}$. P_{jj}), where P_{ii} and P_{jj} are
nce between the filtered data
n 500 to 2000 Hz for the *f–k*,
'low' coherence level (≤ 0.8)
z, because the piezo-electric
in this frequency band. In
spectrum that has little more
wavefield with two octaves.
transform of the coherence
eigenvector filter maximum
wavelet that is impulse-like,

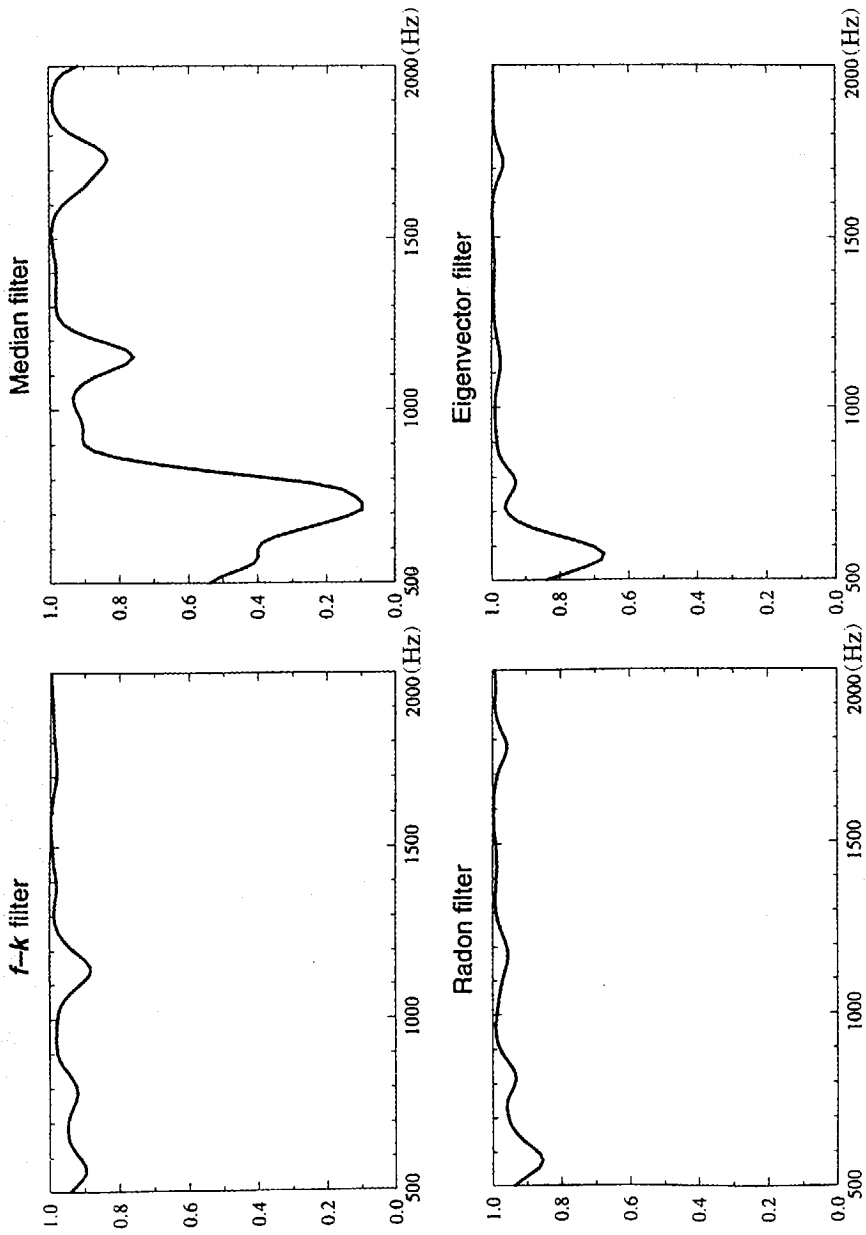

Figure 6. Coherence functions in the frequency domain between the initial data and the output of each type of multichannel filter.

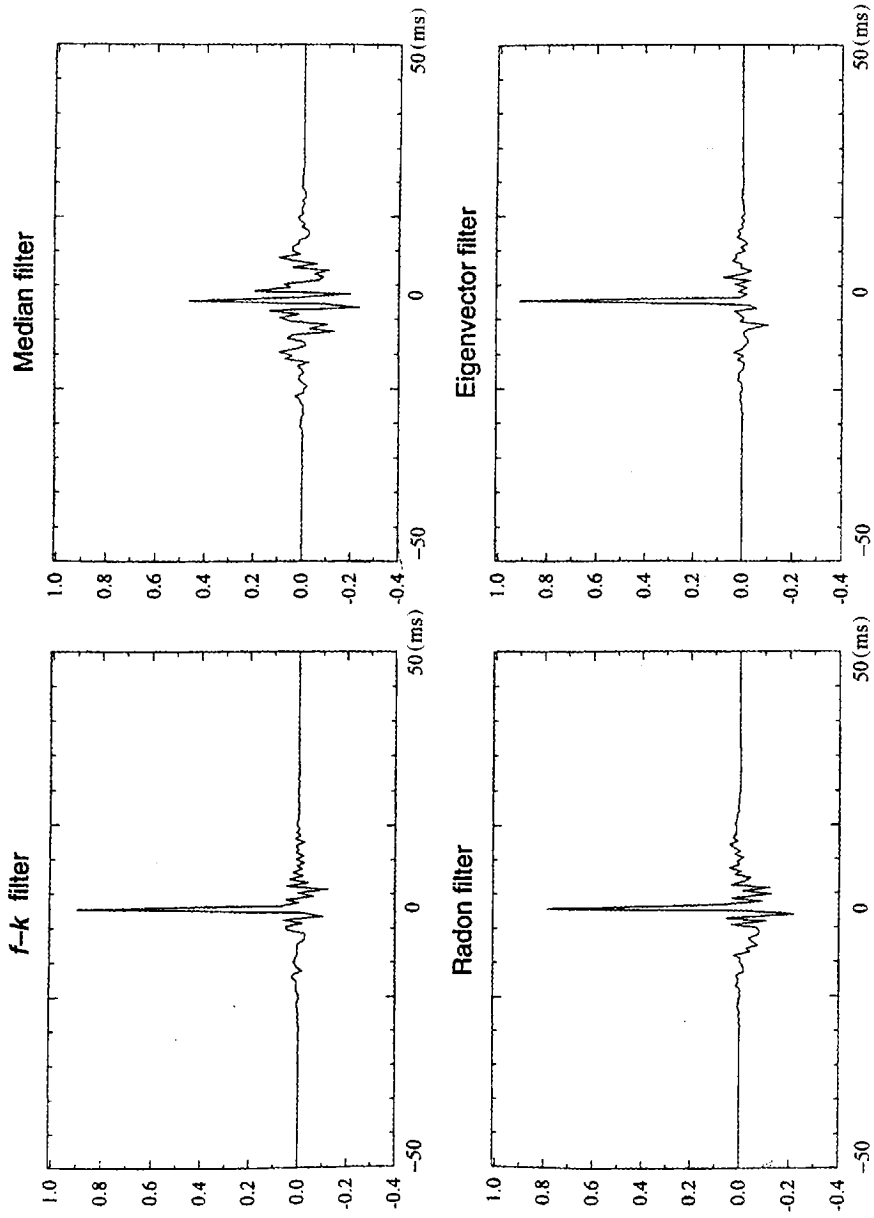

Figure 7. Coherence functions in the time domain between the initial data and the output of each type of multichannel filter. (Vertical axes are normalized by the eigenvector filter maximum value.)

with small sidelobes, while the median filter, with its reduced octave range, has very high sidelobes.

An entire cross-well data set case (large well spacing)

In order to compare the performance of different multichannel filters on an entire cross-well data set, we used data collected by TomoSeis Inc. using a piezo-electric source with an improved spectrum (more output between 200 and 500 Hz) and hydrophone receivers between wells spaced 990 ft apart at British Petroleum's Devine test site. Previous cross-well studies performed at the Devine site demonstrated the existence of high-frequency energy and reflections from major stratigraphic boundaries (Harris 1988; Lazaratos *et al.* 1993; Miller *et al.* 1993; Schuster and Sun 1993). Anisotropy and high velocity contrast were shown to complicate the reflection imaging process. The well spacing of 990 ft is a typical well spacing in US oilfields. The

Figure 7. Coherence functions in the time domain between the initial data and the output of each type of multichannel filter. (Vertical axes are normalized by the eigenvector filter maximum value.)

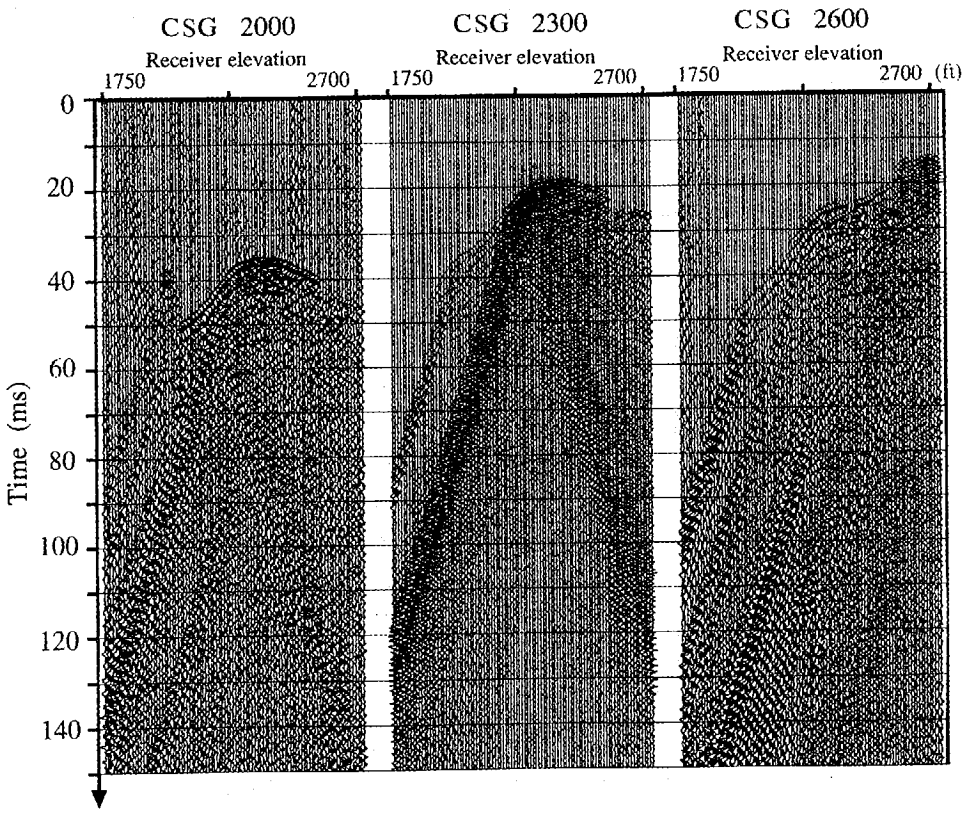

Figure 8. Initial data obtained in three common-source gathers with the source located at 2000, 2300 and 2600 ft, respectively. The receiver elevation ranges from 1700 to 2700 ft.

larger well spacings and the relatively limited vertical aperture of the survey created much wider angles of incidence than were used in the McElroy data set, resulting in a direct arrival that was sometimes difficult to identify. Figure 8 shows three different representative common-source gathers, where the source is located at 2000, 2300 and 2600 ft, respectively. Along with the P-wave direct arrival, the major interference consisted of tube-wave arrivals. S-wave and converted S-wave arrivals were very weak in this data set. The 5 ft sampling of sources and receivers created a data set that was substantially more aliased than the McElroy data set. Tube waves in common-source or common-receiver space cross the spatial Nyquist axis at a frequency of about 450 Hz, resulting in several wraps across the f–k plane in the band of interest (200–2000 Hz).

Figure 9 shows a common-mid-depth gather from the centre of the survey (2300 ft). The common-mid-depth domain (Rector *et al.* 1994) is a useful domain in which to identify reflections because, for a constant velocity, the upgoing and downgoing reflection moveouts are zero. A strong upgoing P-wave reflection from what we believe to be the base of the Austin Chalk is apparent in the unprocessed common-mid-depth gathers.

We used a processing similar to that used at McElroy (Rector *et al.* 1995) to extract upgoing P-wave reflections from this cross-well data set. However, we modified the

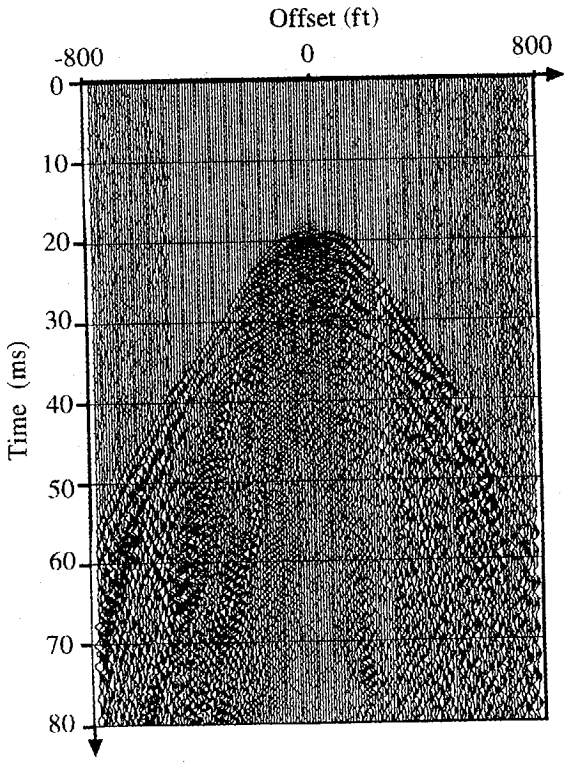

Figure 9. Common-mid-depth gathers at 2300 ft. Offset values range from −800 to 800 ft.

erture of the survey created
Elroy data set, resulting in a
gure 8 shows three different
is located at 2000, 2300 and
val, the major interference
vave arrivals were very weak
s created a data set that was
waves in common-source or
frequency of about 450 Hz,
of interest (200–2000 Hz).
entre of the survey (2300 ft).
useful domain in which to
ng and downgoing reflection
m what we believe to be the
mmon-mid-depth gathers.
Rector *et al.* 1995) to extract
However, we modified the

s range from −800 to 800 ft.

sequence to remove upgoing and downgoing tube waves, as well as the direct arrival signals. We did not apply filtering to shear arrivals. We experimented with the different filters for the different arrivals. With respect to the preprocessing, we found that arrival alignment and scaling was necessary for substantial attenuation of the undesired arrivals. We picked and aligned both the direct arrivals and the tube waves prior to filtering.

We compared the different filters by applying one type of filter (median, f–k pie-slice, radon, eigenvector) to the entire wavefield separation sequence which consisted of a sequence of five separate filters.

1 Tube-wave upgoing and downgoing arrivals removal in common-source space.
2 Tube-wave upgoing and downgoing arrivals removal in common-receiver space.
3 P-wave direct arrivals removal in common-receiver space.
4 P-wave direct arrivals removal in common-source space.
5 P-wave direct arrivals removal in common-offset space.

For each filter pass, we aligned and equalized the undesired wave. We designed the filter parameters as in the McElroy study. We found that the eigenvector filter gives the best result based upon its ability to attenuate the tube waves without putting a notch in a frequency spectrum of the upgoing P-wave reflection. In Fig. 10, a common-source gather located at 2000 ft is plotted in the f–k domain before tube-wave attenuation filtering. Very strong tube waves are detected and wrap across the upgoing energy (apparent velocity of about 20 Kft/s) at a frequency of about 900 Hz for upgoing tube waves, 1100 Hz for downgoing tube waves. The upgoing and downgoing tube waves wrap across the upgoing reflections again at about 1400 Hz and 1550 Hz, respectively. In each wrap, the apparent velocity of the tube wave is not constant over the range of source depths. After alignment and normalization of upgoing tube waves, we use a median filter to attenuate upgoing tube waves. Notches appear in the upgoing reflection spectrum crossing points (Fig. 11). Similar results were obtained with the f–k and radon filters. The eigenvector filter, based on arrival amplitude as well as moveout, avoids notch effects and passes the reflection arrival in the overlapping frequency range (Fig. 12). Due to the large amplitude difference between the tube waves and the upgoing reflection, the eigenvector filter is able to work past the limits of aliasing. This result holds important implications for cross-well and/or VSP imaging. Unfortunately initial analysis of the eigenvector-filtered results also showed that significant amounts of reflection energy were attenuated using the eigenvector filter. When we reduced the percentage of energy removed by the eigenvector filter, we began to see residual tube waves, indicating that some eigenvectors contain undesired tube-wave arrivals along with reflection arrivals.

These results indicated that, to avoid removing some of the reflection energy of interest, we needed to 'constrain' the eigenvector filter. The constrained eigenvector filter would only be able to attenuate a narrow range of spatial frequencies. We constructed a constrained eigenvector filter by the following process. First, we computed the eigenimage of the aligned tube waves. Then, we spatially filtered this eigenimage with a mild 3-trace mix. Finally we subtracted this mixed eigenimage from

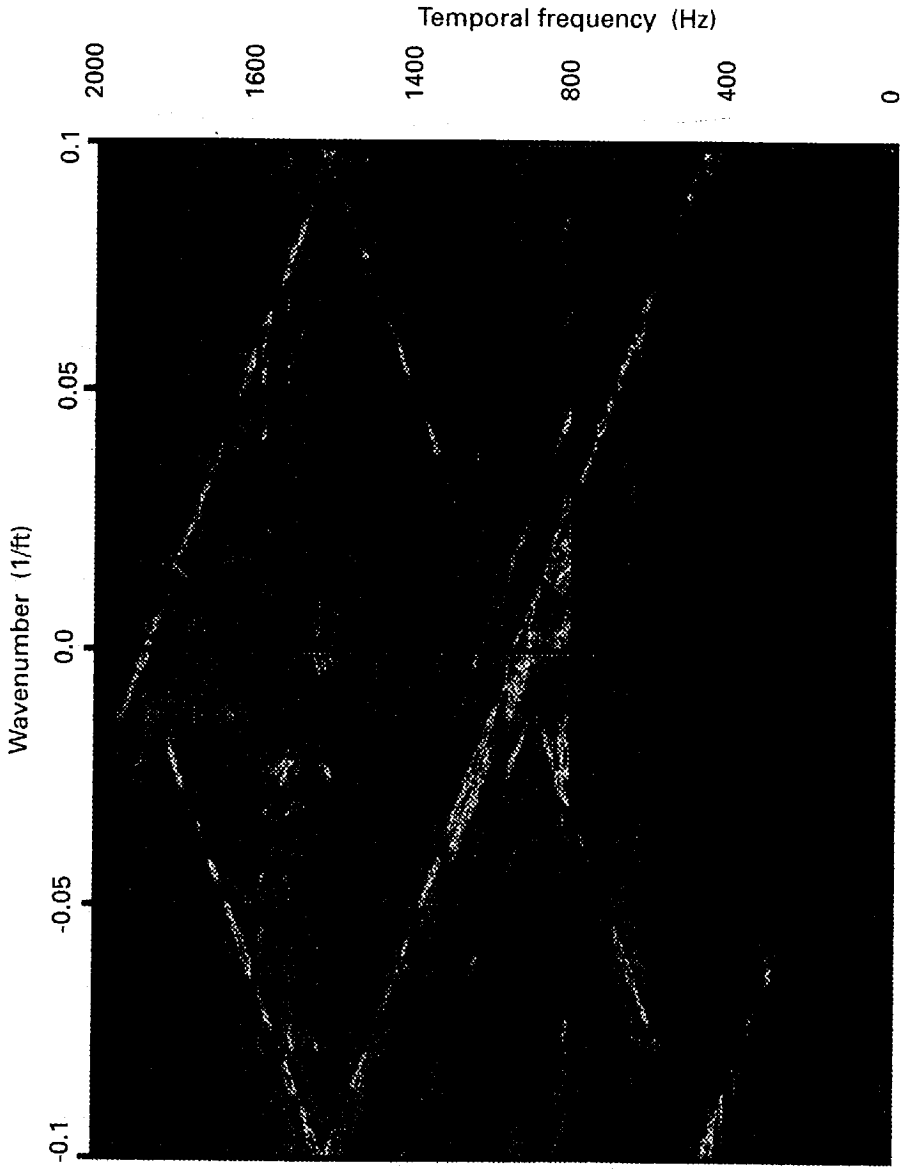

Figure 10. *f–k* spectrum of the common-source gather data (at 2000 ft). Tube-wave arrivals are clearly visible.

Figure 10. f–k spectrum of the common-source gather data (at 2000 ft). Tube-wave arrivals are clearly visible.

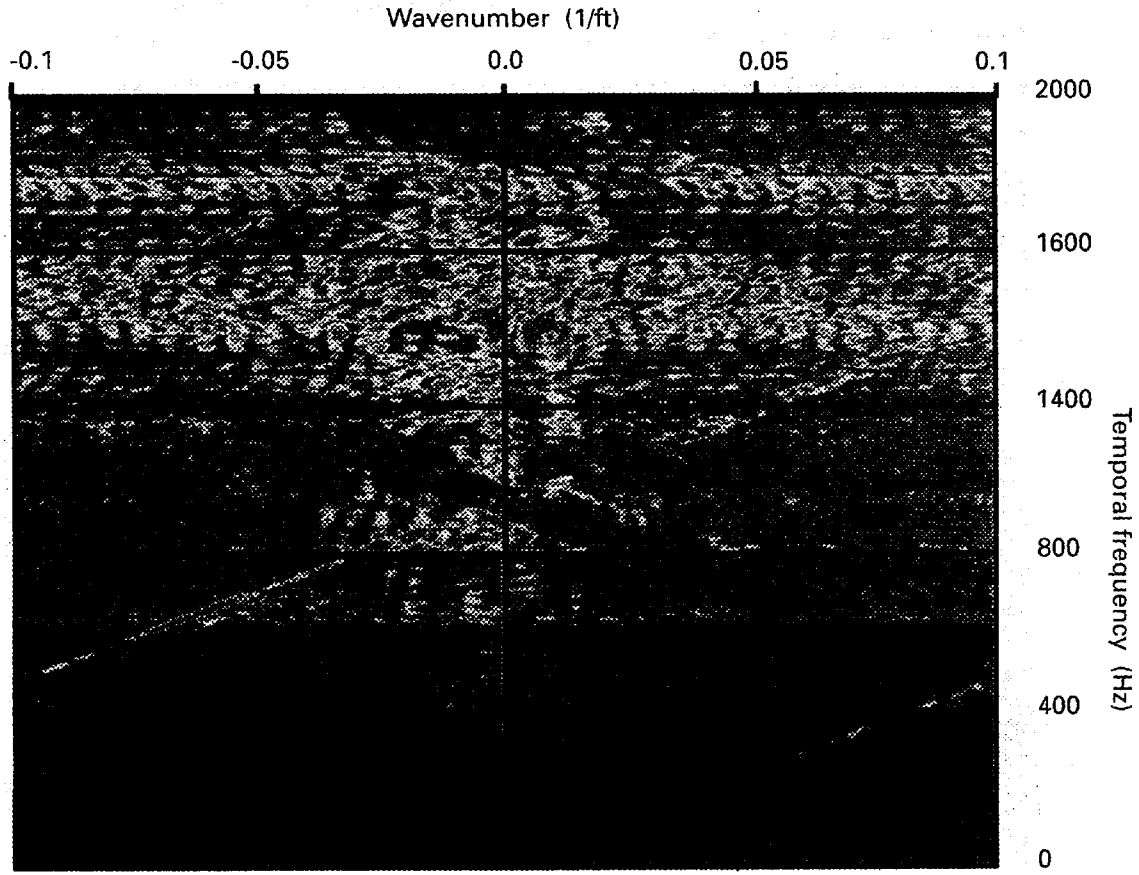

Figure 11. f–k spectrum of the common-source gather data (at 2000 ft) after alignment based on the upgoing tube-wave velocity and removal of the tube-wave arrivals by the median filter.

Geophysical Prospecting, 47, 611–636

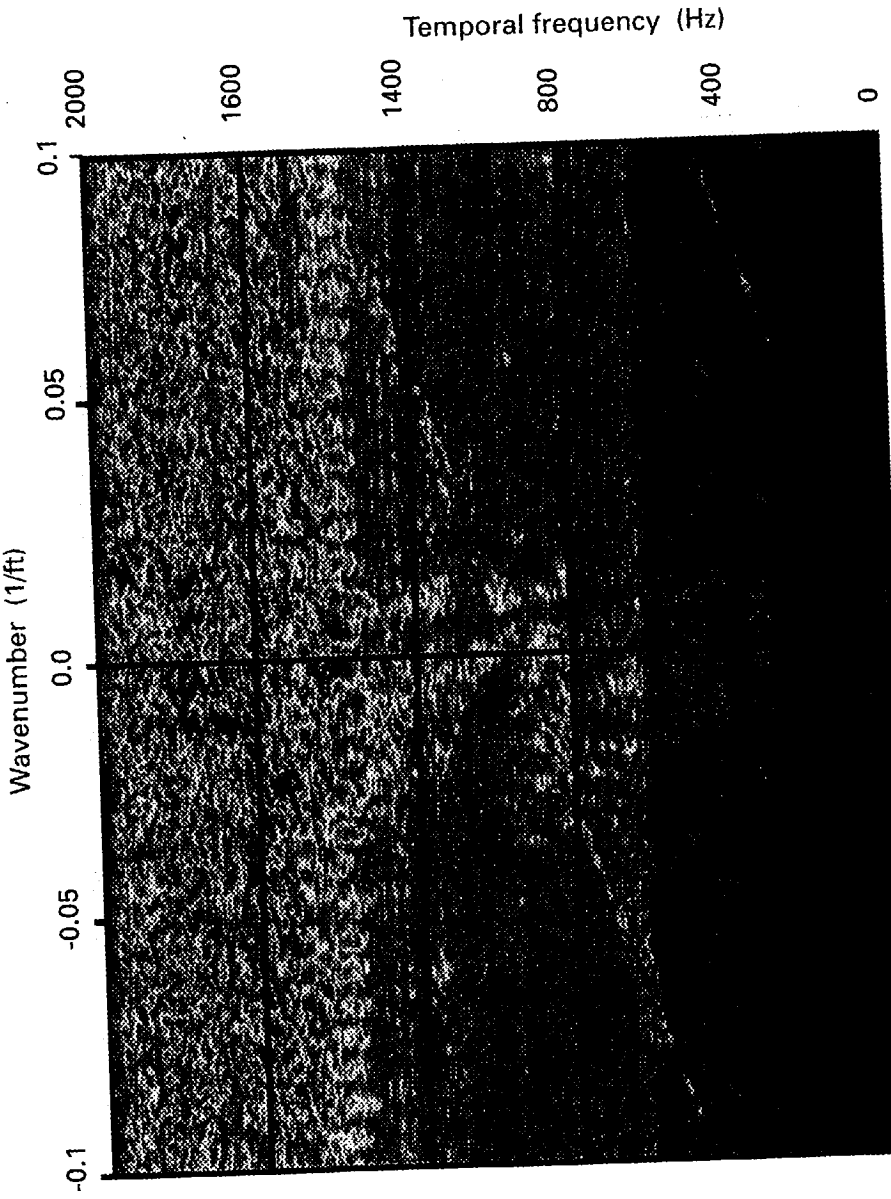

Figure 12. f–k spectrum of the common-source gather data (at 2000 ft) after alignment based on the upgoing tube-wave velocity and removal of the tube-wave arrivals by the eigenvector filter.

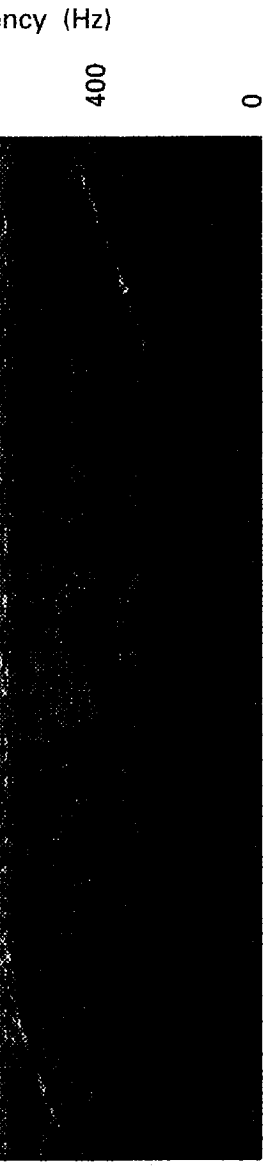

Figure 12. *f–k* spectrum of the common-source gather data (at 2000 ft) after alignment based on the upgoing tube-wave velocity and removal of the tube-wave arrivals by the eigenvector filter.

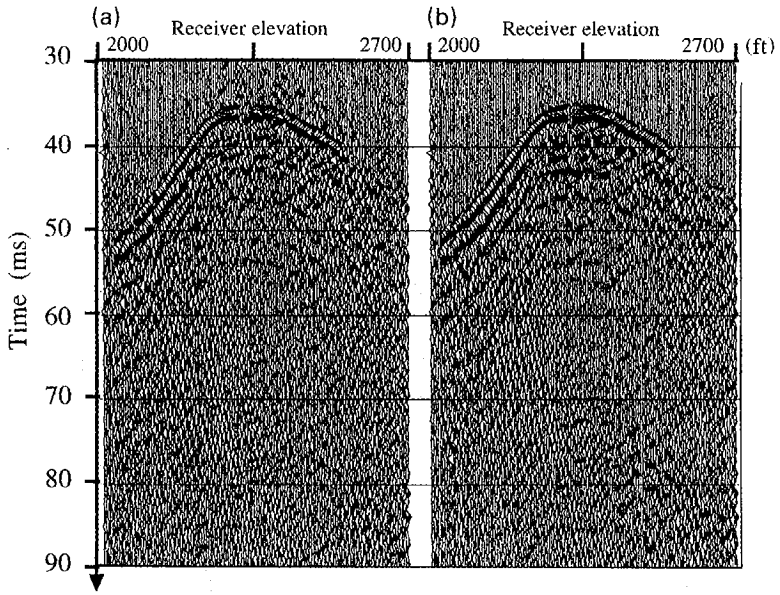

Figure 13. Results obtained using (a) standard eigenvector filters and (b) constrained eigenvector filters.

the original data. Figure 13 shows the results obtained using the standard eigenvector filter compared with those obtained using the constrained eigenvector filters. We see that reflections are clearer for the constrained eigenvector-filtered data than for the standard eigenvector-filtered data. Note how the tube-wave noise has been attenuated without notching effects of spatial filters or the attenuation of reflection energy in the eigenvector-filtered data.

In order to compare processing, we applied the entire wavefield separation processing sequence using the different filter formulations (median, *f–k* pie-slice, radon and constrained eigenvector) to the entire data set. Results (Figs 14a–c) are shown for a common-mid-depth image related to Fig. 9. Figure 14a shows the result after wavefield separation using a 9-trace median filter for every multichannel filtering operation. Figure 14b shows the data after wavefield separation using an *f–k* pie-slice filter with ± 80 Kft/s for every multichannel operation. Figure 14c shows the result after using the constrained eigenvector filter to attenuate the aliased tube waves and a radon filter to attenuate the unaliased direct arrivals. As in the comparison of the common-receiver gather data, it is difficult to identify which gather is superior. Focusing on the time window ranging from 20 to 30 ms, we can see that for median filter processing, no important reflectors are clearly visible on the entire designing area. For *f–k* pie-slice processing, reflectors are difficult to pick. Removing aliased tube waves by constrained eigenvectors and using radon filters to remove the P-wave direct arrivals gives strong reflectors which can be easily picked. Furthermore, the median-

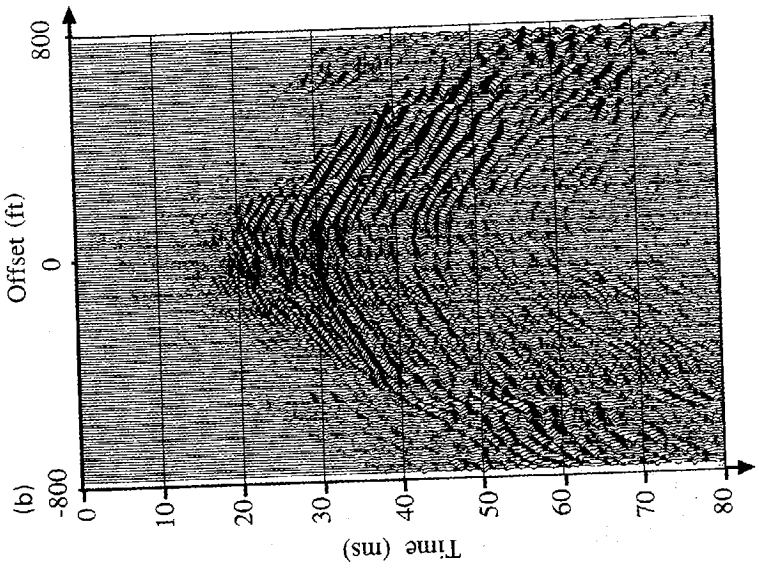
(b)
Offset (ft)
800
0
-800
0
10
20
30
40
50
60
70
80
Time (ms)

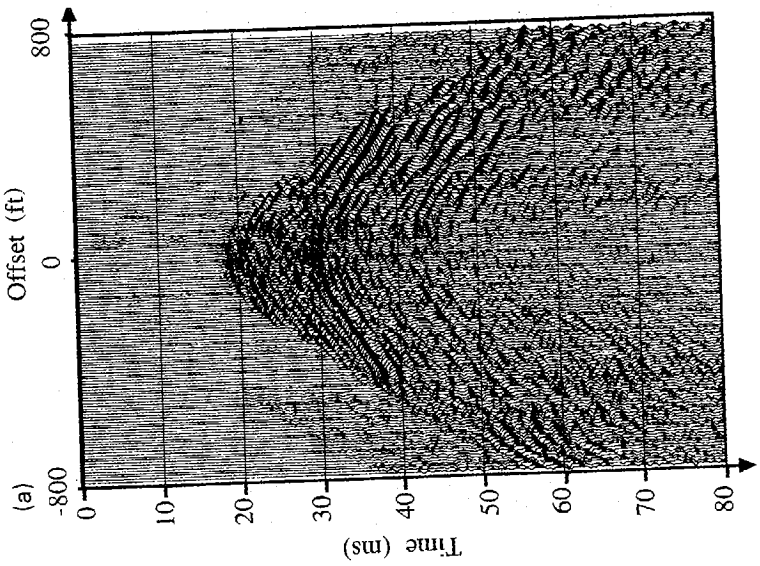
(a)
Offset (ft)
800
0
-800
0
10
20
30
40
50
60
70
80
Time (ms)

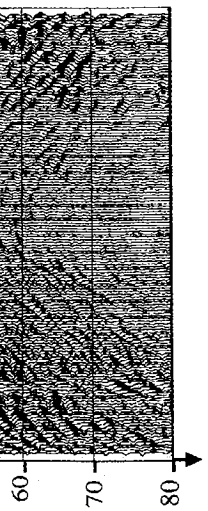

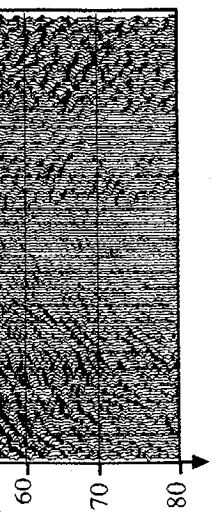

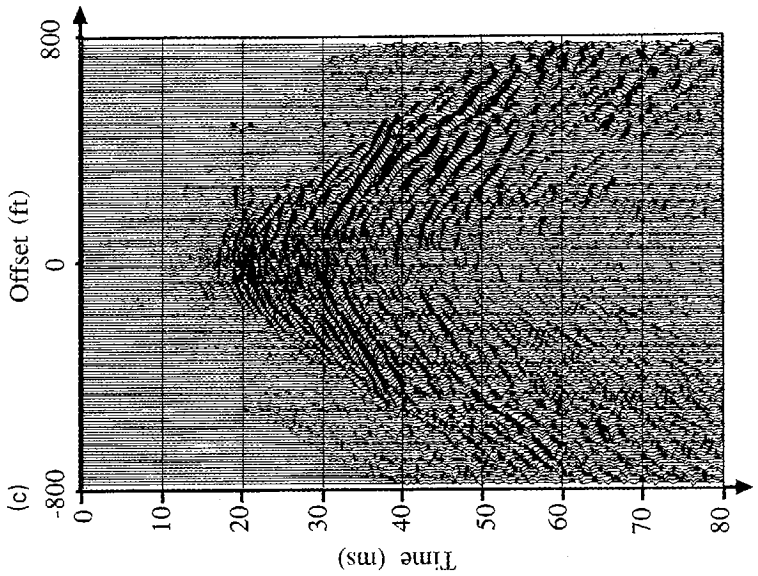

Figure 14. (a) Result obtained from the entire wavefield separation processing sequence using a median filter for each multichannel operation. (b) Result obtained from the entire wavefield separation processing sequence using an f–k pie-slice filter for each multichannel operation. (c) Result obtained from the entire wavefield separation processing sequence using the constrained eigenvector filter to attenuate aliasing tube-wave arrivals and a radon filter to remove unaliased direct arrivals.

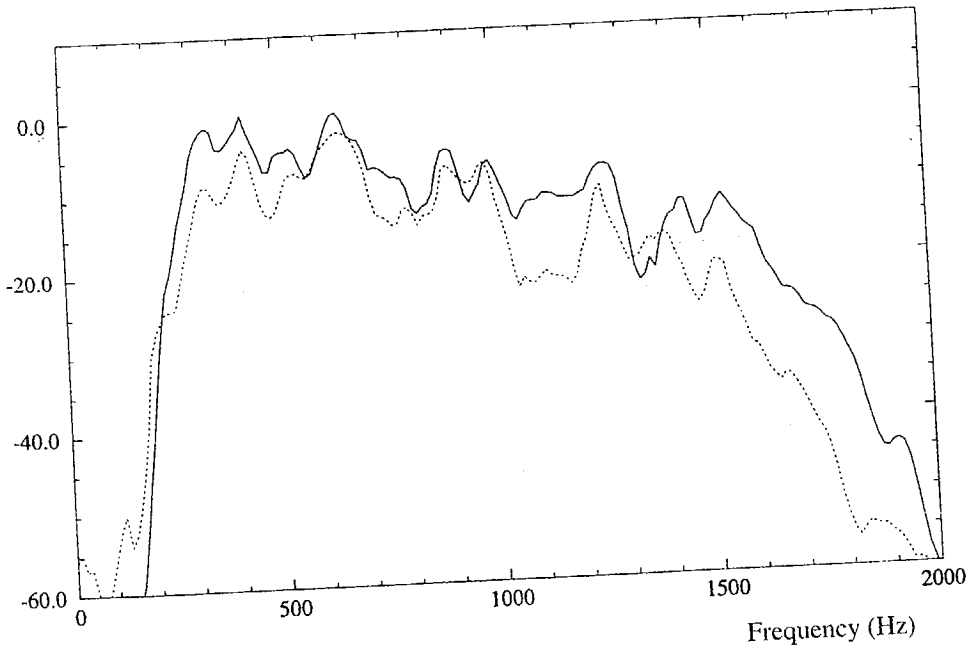

Figure 15. Comparison between median filter stacked spectrum data and constrained eigenvectors stacked data. Solid line: constrained eigenvectors; dotted line: median process.

filtered results appear to produce reflection energy with a ringer appearance, possibly indicative of a loss of low-frequency energy.

We evaluated the signal quality of the filtered common-mid-depth gathers by stacking the data after correcting for the residual moveout computed along the large reflector located between 30 and 40 ms. Figure 15 shows the stacked spectrum. Note that the data from Fig. 14c have the largest broadband spectrum. We can see the tube-waves notches introduced by the pure spatial filtering at 950, 1100 and 1500 Hz. We can also see the loss in low frequency produced by the median filter. From the stacked spectrum analysis, it appears that the choice of wavefield separation filter is quite important to the quality and post-separation bandwidth of the reflection energy.

Conclusions

We have shown that arrival alignment and amplitude scaling are important for multichannel filtering and that the choice of the multichannel filter and filter parameters is critical to the wavefield separation of cross-well data. We found that spatial aliasing creates situations where the application of purely spatial filters will create notches in the frequency spectrum of the desired reflection arrival. Median filters exhibited the added problem of attenuating the lower frequencies of the desired signal. Eigenvector filters were found to work past the limits of aliasing, but were found

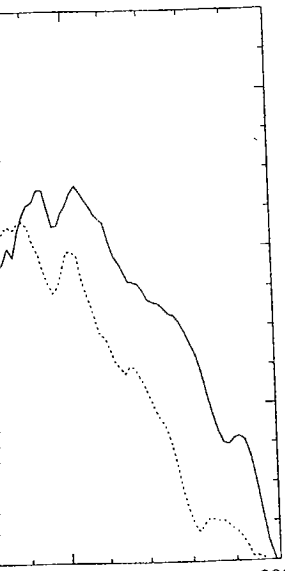

pectrum data and constrained
dotted line: median process.

a ringer appearance, possibly

nmon-mid-depth gathers by
out computed along the large
s the stacked spectrum. Note
pectrum. We can see the tube-
t 950, 1100 and 1500 Hz. We
iedian filter. From the stacked
field separation filter is quite
of the reflection energy.

de scaling are important for
multichannel filter and filter
ross-well data. We found that
n of purely spatial filters will
red reflection arrival. Median
ower frequencies of the desired
nits of aliasing, but were found

to be strongly dependent on the ratio of undesired to desired signal amplitude. For data where the desired and undesired signals had comparable amplitudes, the eigenvector filters were not useful in wavefield separation. As a result of these observations, we developed a new type of multichannel filter which combined the best characteristics of spatial filters and eigenvector filters. We call this filter a constrained eigenvector filter. Results from application of the constrained eigenvector filter to the entire cross-well data set are superior to both the spatial and standard eigenvector filter results.

Acknowledgements

This work was supported by CRADA #TSI-201-94 with TomoSeis Inc., as part of a small business innovation research grant funded by the US Department of Energy, and was also funded by a 'Region Rhones-Alpes Bourse d'Excellence' from France.

References

Duncan G. and Beresford G. 1995. Median filter behaviour with seismic data. *Geophysical Prospecting* **43**, 329–345.

Embree P., Burg J.P. and Backus M.M. 1963. Wide band velocity filtering – the pie-slice process. *Geophysics* **28**, 948–974.

Esmersoy C. 1990. Inversion of P and SV waves from multicomponent offset vertical seismics profiles. *Geophysics* **55**, 39–50.

Foster D.J. and Mosher C.C. 1992. Suppression of multiple reflections using the Radon transform. *Geophysics* **57**, 386–395.

Freire S.L.M. and Ulrych T.S. 1988. Application of singular value decomposition to vertical seismic profiling. *Geophysics* **53**, 778–785.

Glangeaud F. and Mari J.L. 1994. *Wave Separation*. Institut Francais du Pétrole and Technips Eds.

Hardage B.A. 1985. *Vertical Seismic Profiling – Part 1, Principles*. Pergamon Press, Inc.

Hardage B.A. 1992. *Cross-Well Seismology and Reverse VSP*. Geophysical Press.

Harris J.M. 1988. Cross-well seismic measurements in sedimentary rocks. 58th SEG meeting, Anaheim, USA, Expanded Abstracts, 147–150.

Harris J.M., Nolen-Hoeksema R., Langan R.T., Van Schaack M., Lazaratos S.K. and Rector J.W., III 1995. High resolution cross-well imaging of a West Texas carbonate reservoir, part 1: Project summary and interpretation. *Geophysics* **60**, 667–681.

Lazaratos S.K., Rector J.W., III, Harris J.M. and Van Schaack M. 1993. High resolution cross-well imaging: Potentials and technical difficulties. *Geophysics* **58**, 1270–1280.

Mars J.M. and Rector J.W., III 1995. Constrained eigenvectors: A means to separate aliased arrivals. 62nd SEG meeting, Houston, USA, Expanded Abstracts, 49–52.

Miller R.D., Pullan S.F., Steeples D.W. and Hunter J.A. 1993. Field comparison of shallow seismic sources near Chino, California. *Geophysics* **57**, 693–709.

Rector J.W., III, Lazaratos S.K., Harris J.M. and Van Schaack M. 1994. Multidomain analysis and wavefield separation of cross-well seismic data. *Geophysics* **59**, 27–35.

Rector J.W., III, Lazaratos S.K., Harris J.M. and Van Schaack M. 1995. High resolution cross-well imaging of a West Texas carbonate reservoir, part 3: Wavefield separation of reflections. *Geophysics* **60**, 692–701.

Rector J.W., III and Mars J. 1995. Preconditioning and analysis of different wavefield separation techniques. 57th EAEG conference, Glasgow, Scotland, Extended Abstracts, B052.

Rowbotham P.S. and Goulty N.R. 1994. Wavefield separation by 3-D filtering in crosshole seismic reflection processing. *Geophysics* **59**, 1065–1071.

Schuster G.T. and Sun Y. 1993. Wavelet filtering of tube and surface waves. 63rd SEG meeting, Washington, DC, USA, Expanded Abstracts, 25–28.

Seeman B. and Horowicz L. 1983. Vertical seismic profiling: separation of upgoing and downgoing acoustic waves in a stratified medium. *Geophysics* **48**, 555–568.

Van Schaack M., Rector J.W., III, Lazaratos S.K. and Harris J.M. 1995. High resolution cross-well imaging of a West Texas carbonate reservoir, part 2: Wavefield modelling and analysis. *Geophysics* **60**, 682–691.

Yilmaz O. 1987. *Seismic Data Processing*. SEG, Tulsa, OK.